ACS MATERIALS LETTERS

www.acsmaterialsletters.org

LETTER

In Situ Reprogrammable Magnetic Microrobots

Guohonghao Zeng,[▽] Hemin Pan,[▽] Maxim A. Kurochkin, Yang Zong, Songyu Xiong, Jinbo Yang, Minjie Xi, Yu Mei, Yongfeng Mei, Xiang-zhong Chen,* and Jizhai Cui*

Cite This: *ACS Materials Lett.* 2025, 7, 3943−3951

Read Online

ACCESS | Metrics & More | Article Recommendations | Supporting Information

ABSTRACT: **Programmability is essential for magnetic microrobots to achieve adaptive and multifunctional behaviors. However, most existing systems lack reconfigurability after deployment. Here, we present a reprogrammable microrobot platform based on nickel nanowires of distinct diameters embedded in SU-8, leveraging the difference in their coercivities to enable *in situ* magnetization switching. A fast, purely magnetic reprogramming strategy is developed, allowing the selective reversal of magnetization states without thermal or structural changes. We systematically explore the effects of ramp time, magnetic field strength, and microrobot geometry on reprogramming success and demonstrate six distinct deformation and locomotion modes in a multisegment robot. The scalable UV photolithography-based fabrication process ensures a high yield and design flexibility. This work provides a generalizable and efficient approach toward reprogrammable microrobotic systems with potential for future applications in dynamic environments such as biomedical actuation or soft robotic manipulation.**

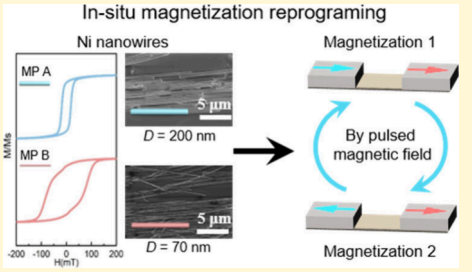

Microrobots are artificial miniaturized devices capable of performing programmed tasks,[1−4] with promising applications in fields such as biomedicine[5−9] and environmental monitoring.[10] Among various microrobots driven by different energy sources,[11−19] magnetically actuated microrobots have attracted attention due to their ability to achieve precise, noncontact, and remote 3D manipulation at micro- and nanoscale. To enable intelligent and adaptable functionalities, such as grasping, folding, swimming, or directional bending, it is essential for magnetic microrobots to exhibit programmability − the ability to undergo complex and controllable deformations in response to external magnetic stimuli. Such programmability is typically encoded through design parameters including geometry, spatial distribution of magnetic materials, and magnetic anisotropy.[20−22] However, in most existing systems, the programmed deformation behavior is fixed once fabrication is complete, rendering the microrobot incapable of adaptation after deployment.

In contrast, reprogrammability refers to the ability to modify a microrobot's magnetization state after its deployment, thereby enabling a switch to entirely new deformation modes under the same external magnetic field. This capacity allows a single microrobot to adapt its behavior dynamically without changing the applied field, which is crucial for executing adaptable, multifunctional tasks in dynamic or uncertain environments. Several reprogramming strategies have been proposed, such as thermally assisted softening of the matrix material for realignment of magnetic particles[23] or thermally induced demagnetization followed by remagnetization of embedded magnetic particles.[24] However, these methods often require multiple energy inputs, involve slow physical processes, and introduce extra complexity into the system. As a result, the reprogramming speed is limited, making such approaches unsuitable for tasks that demand rapid adaptability or swift transitions between different functional states.

While existing methods (e.g., thermal, chemical, and uniform magnetization) enable basic locomotion or deformation modes, their limited reconfigurability (1−3 modes) and slow reprogramming speeds (seconds to minutes) hinder their utility in complex tasks such as multistep drug delivery or dynamic environmental adaptation. Here, we propose a magnetic reprogramming strategy based on nanowire arrays with coercivity gradients, achieving six independently controllable modes (e.g., segment-specific bending, synchronized twisting, and rolling) via purely magnetic modulation, surpassing the functional limitations of thermal/chemical approaches. Furthermore, our method supports real-time mode transitions with millisecond-scale switching speeds, offering a 1000-fold acceleration over state-of-the-art techni-

Received: July 31, 2025
Revised: October 29, 2025
Accepted: October 30, 2025

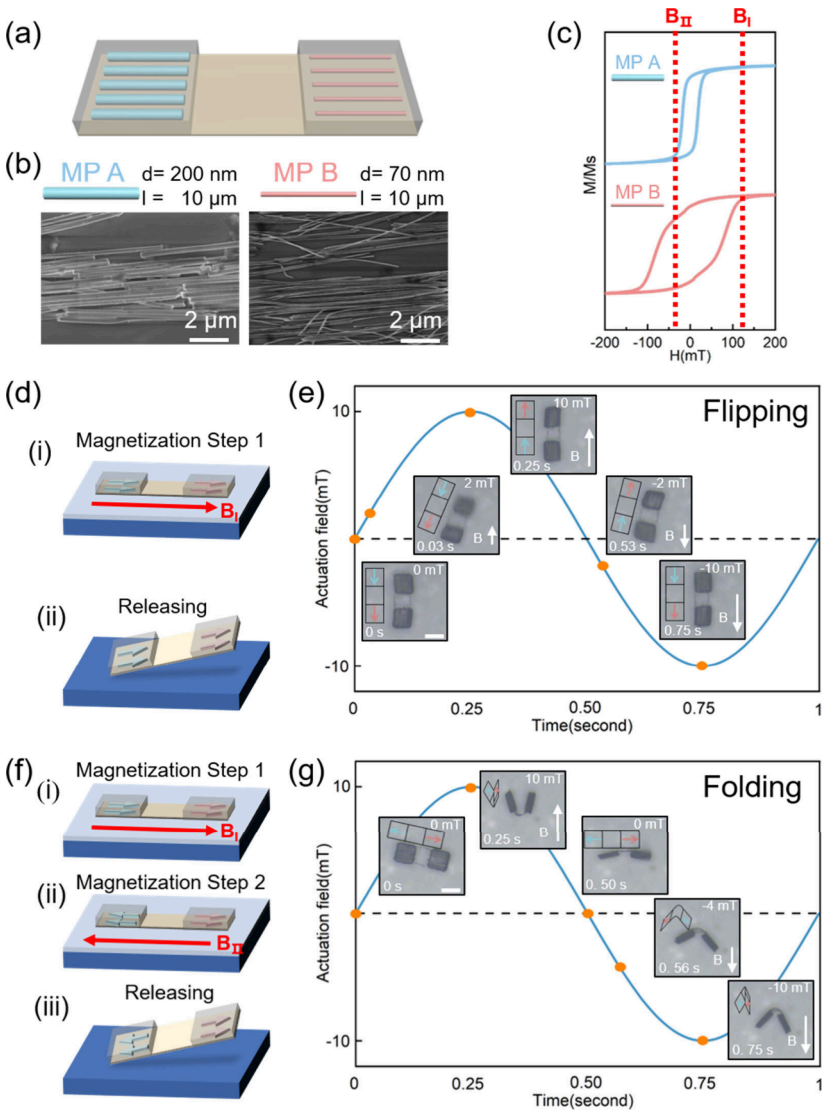

Figure 1. (a) Morphology of the reprogrammable magnetic microrobot (RP-MR). SEM images (b) and magnetic hysteresis loops (c) of nickel nanowires. (d) Schematic illustration of the microrobot initially magnetized in the parallel direction (i) and then released (ii). (e) Motion of the microrobot under a sinusoidal oscillating magnetic field after parallel magnetization and subsequent release. (f) Schematic illustration of the microrobot premagnetized in the parallel direction (i), then remagnetized in the antiparallel direction (ii), and subsequently released (iii). (g) Motion of the microrobot under a sinusoidal oscillating magnetic field after antiparallel magnetization and release.

ques, enabling novel applications in biomedicine and unstructured environments. By embedding two types of nickel nanowires, with different diameters and thus distinct coercivities, into SU-8 matrices, we enabled selective magnetization through controlled magnetic field. This allows microrobots to switch their magnetic states and thereby access distinct deformation and locomotion modes under the same external magnetic fields. Being different from the previously reported work using complex and costly fabrication techniques such as electron-beam lithography,[20,25] our approach is based on a scalable and low-cost UV photolithography process. This method allows batch fabrication of reprogrammable magnetic microrobots with magnetic units as small as 100 μm and offers high flexibility in robot geometry design, opening new possibilities for adaptive microrobotic systems in dynamic environments.

Figure 1a shows the basic structure of the reprogrammable magnetic microrobot (RP-MR), which consists of three main components: two SU-8-based magnetic panels embedded with well-aligned nickel nanowires of distinct diameters—200 nm for Magnetic Particles A (MP A) and 70 nm for Magnetic Particles B (MP B)—and a flexible hinge made of poly(*N*-isopropylacrylamide) (pNIPAM).[26] Nickel nanowires were chosen over nanoparticles due to their intrinsic magnetic anisotropy and the ability to achieve distinct coercivity values based on diameter, enabling precise, directional magnetic switching for multimodal actuation. Both MP A and MP B have a fixed length of 10 μm and are uniformly dispersed in SU-8 at a concentration of 2 wt %. The fabrication process is shown in Scheme 1, and the fabrication details are illustrated in the Supporting Information (I. Fabrication of nickel nanowires and II. Fabrication of magnetically reprogrammable microrobots). The pNIPAM hinge connects the two magnetic panels and allows for flexible deformation. Each magnetic panel of the RP-MR measures 100 × 100 μm, and the hinge length of pNIPAM is 100 μm. Using UV photolithography, an 8 × 8

https://doi.org/10.1021/acsmaterialslett.5c01084
ACS Materials Lett. 2025, 7, 3943−3951

Scheme 1. (a) Fabrication Process of Nickel Nanowires and (b) Fabrication Process of Magnetically Reprogrammable Microrobots

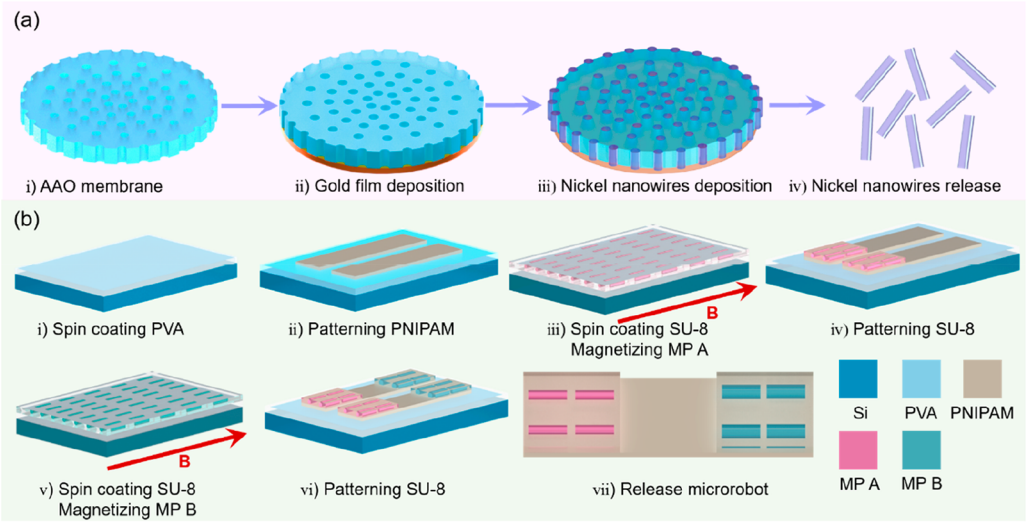

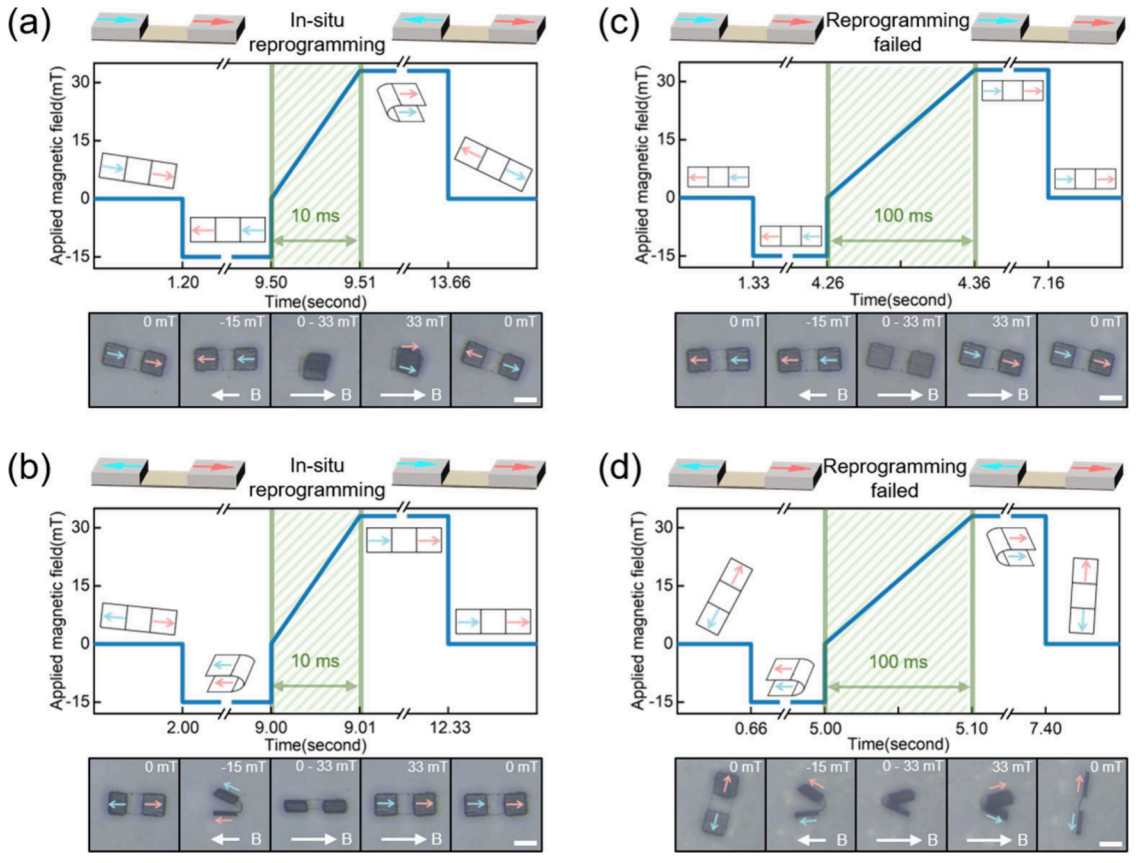

Figure 2. Successful reprogramming of the microrobot was achieved after a magnetic field raising time of 10 ms in both the parallel (a) and antiparallel (b) initial magnetization states. When the raising time was extended to 100 ms, reprogramming failed in both the parallel (c) and antiparallel (d) initial magnetization states.

array of RP-MRs was fabricated on a 1.5 × 1.5 cm silicon substrate. The morphology of the resulting RP-MRs is shown in Figure S1.

Figure 1b presents scanning electron microscopy (SEM) of MP A and MP B, revealing smooth surfaces and a uniform length and diameter. The nanowires were fabricated by using a template-assisted electrodeposition, as detailed in Scheme 1a. As one-dimensional ferromagnetic structures, nickel nanowires exhibit strong magnetic shape anisotropy, leading to significantly different magnetization behaviors along their axial and radial directions. Crucially, their coercivity along the long axis is diameter-dependent—thinner nanowires exhibit higher coercivity. Magnetic characterization was performed exclusively on finalized SU-8/nickel nanowires composites to capture operational-state properties. Specifically, the measurements were performed using a NanoMOKE

https://doi.org/10.1021/acsmaterialslett.5c01084
ACS Materials Lett. 2025, 7, 3943−3951

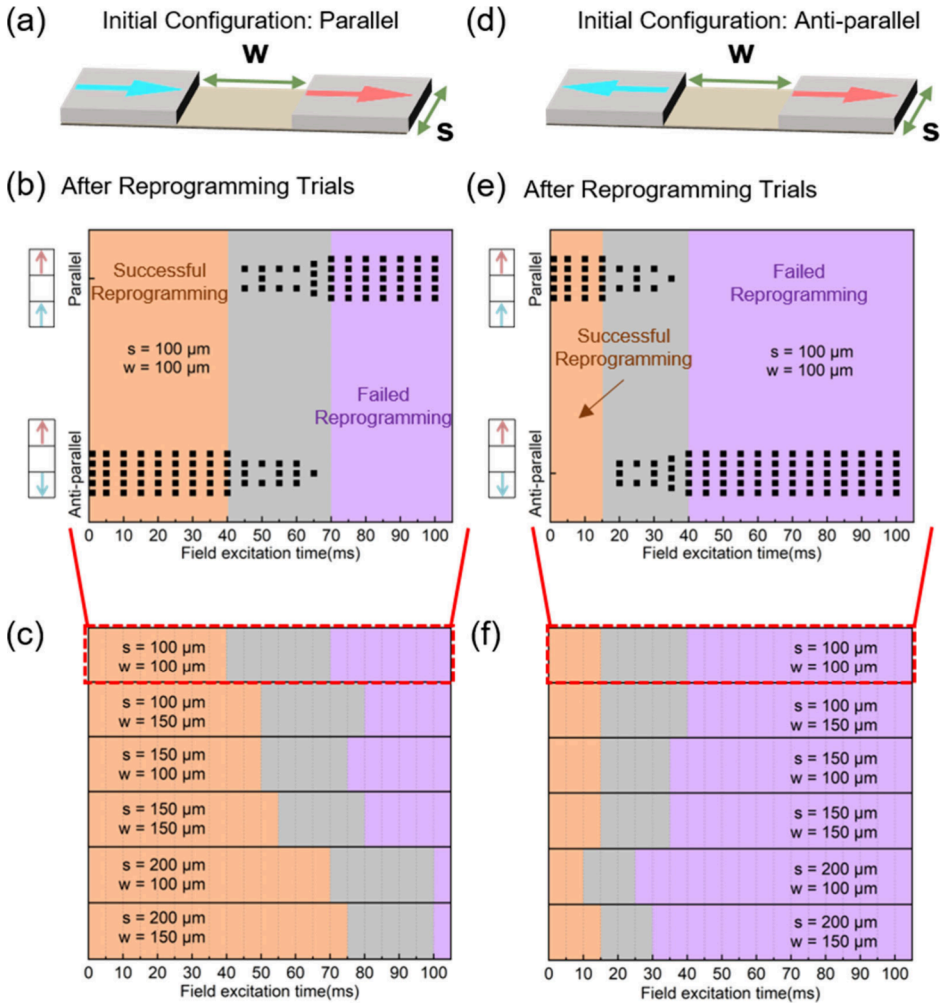

Figure 3. (a) Geometric parameters of the microrobot in parallel magnetization states. Reprogramming ramp time−response diagrams of a microrobot with panel size of 100 μm, hinge length of 100 μm, and initial parallel magnetization state (b), and for five additional microrobots with varying parameters (c). (d) Geometric parameters of the microrobot in antiparallel magnetization states. Reprogramming ramp time−response diagrams of a microrobot with panel size of 100 μm, hinge length of 100 μm, and initial antiparallel magnetization state (e) and for five additional microrobots with varying parameters (f).

magnetometer on the fabricated microrobot samples, which include the nickel nanowires encapsulated within the SU-8 matrix. As shown in Figure 1c, the coercive field of MP A (200 nm) is 18 mT, whereas that of MP B (70 nm) exhibits a coercivity of 74 mT.

This coercivity contrast enables selective programming and reprogramming of the magnetization states via field-controlled magnetization. After aligning both MP A and MP B along the parallel direction, a strong external magnetic field ($\mathbf{B}_I$ > 74 mT, e.g., 100 mT) fully magnetizes both segments. A subsequent reversed magnetic field $\mathbf{B}_{II}$, applied within the range of 18−74 mT, selectively reverses the magnetization of MP A without altering MP B, thus achieving an antiparallel magnetization configuration. This mechanism enables programmable switching between magnetic states within the same microrobot and, consequently, distinct deformation modes under identical actuation fields, an essential feature of reprogrammability.

Figure 1d−g illustrates the different actuation behavior of two RP-MRs with different magnetic state configuration under the same sinusoidal magnetic field (10 mT, 1 Hz). In the first experiment (Figure 1d,e), both magnetic segments were magnetized in the parallel direction ($\mathbf{B}_I$) prior to being released into deionized (DI) water. Upon applying the actuation field (10 mT, 1 Hz), the RP-MR exhibited flipping motion synchronized with the switching of the external magnetic field, without any relative deformation between the two magnetic panels in the robot (Video S1). Representative snapshots are shown in Figure 1e, corresponding to the time points indicated in red on the field-time plot. In the second experiment (Figure 1f,g), after the initial B_I magnetization, a reversed magnetic field $\mathbf{B}_{II}$ was applied to selectively remagnetize the MP A panel. This generated an antiparallel magnetization configuration. The microrobot was then released into DI water. When actuated under the same sinusoidal field, the RP-MR exhibited a distinct V-shaped folding motion at the hinge, characterized by relative motion between the two panels (Figure 1g and Video S1), confirming the deformation programmability enabled by the magnetic configuration.

We then demonstrated the *in situ* reprogrammability of our RP-MR system (Figure 2a). Initially an RP-MR with both magnetic panels magnetized in the parallel direction was released into the water. Then a static magnetic field of −15

https://doi.org/10.1021/acsmaterialslett.5c01084
ACS Materials Lett. 2025, 7, 3943−3951

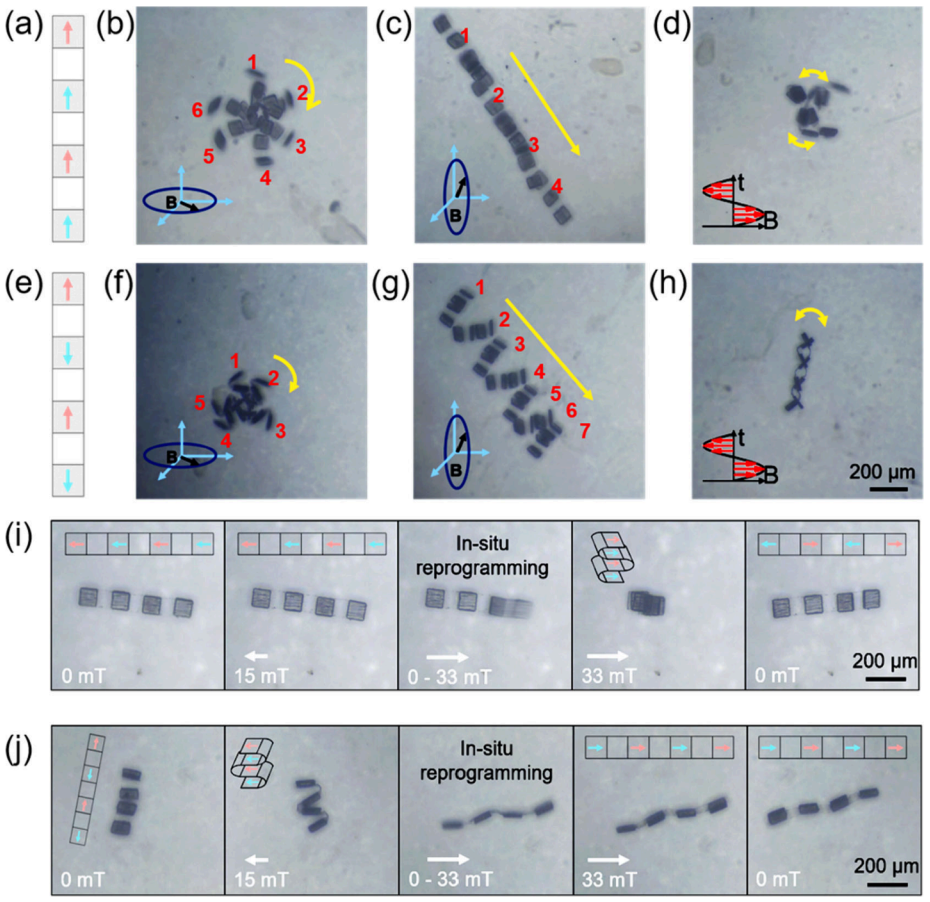

Figure 4. Schematic illustrations of the microrobot with four panels with initial magnetization state of uniform direction (a) and alternating direction state (e), and their responses to an in-plane rotating magnetic field (b), (f), an out-of-plane rotating magnetic field (c), (g), and an oscillating magnetic field (d), (h), respectively. (i) Schematic of *in situ* reprogramming from the uniform to the alternating magnetization state. (j) Scheme of *in situ* reprogramming from the alternating to the uniform magnetization state.

mT was applied to align the microrobot's orientation. Afterward, a magnetic field was ramped from 0 to 33 mT in a short duration (t = 10 ms), completing the reprogramming process. The field strength exceeds the coercivity of the MP A (18 mT) but remains below that of the MP B (74 mT), thereby selectively reversing the magnetization of MP A while preserving that of MP B. This selective switching enables a transformation in the internal magnetic configuration, from parallel to antiparallel, which in turn changes the robot's actuation behavior under the same external magnetic field. The full process is visualized in Video S2, and representative frames of magnetization and deformation states are shown in Figure 2a. The schematic above the frames illustrates the corresponding magnetic configurations before and after reprogramming.

Two key parameters influence the *in situ* programming process: the reprogramming field strength and the field ramping time (t). To investigate the effect of field strength, we fixed the ramping time at t = 10 ms and varied the peak value of the field between 21 and 36 mT. After reprogramming, a low actuating field of 5 or 10 mT was applied to induce deformation, and to evaluate the effect of reprogramming by measuring the bending angle θ. A larger θ corresponds to a greater magnetic moment contrast between the two panels. As shown in Figure S3, bending angle θ reaches its maximum at 33 mT, indicating the optimal reprogramming performance under this condition.

We next examined the effect of the ramping time t. As illustrated in Figure 2a,c, raising t from 10 ms to 100 ms while keeping the peak field constant lead to a complete failure of reprogramming. As shown in Video S2, when the ramp is slow (t = 100 ms), the robot rotates and aligns with the external field before it reaches the coercive field (18 mT). As a result, the nanowires never experience an external field greater than 18 mT that is antiparallel to their original magnetization, rendering them unaffected and un-remagnetized. In other words, under a fixed magnetic field magnitude, a short t enables successful magnetic reprogramming, whereas a longer t fails to. A similar trend is observed for RP-MRs initially magnetized in the antiparallel direction. As demonstrated in Figure 2b,d, rapid ramping (t = 10 ms) enables successful reprogramming of the RP-MR with antiparallel magnetization, while slower ramping fails. A comparison in Video S2 further reveals that the orientation of the RP-MR under a −15 mT magnetic field differs depending on its initial state, which significantly influences the reprogramming outcome.

We further investigated the influence of the ramp time on reprogramming performance for RP-MRs with different initial magnetic configurations (i.e., parallel (Figure 3a) and antiparallel (Figure 3d) states) and geometric parameters. All experiments were conducted at a fixed field amplitude of 33 mT. We first examined RP-MRs with panel size s = 100 μm and hinge length w = 100 μm and varied the ramp time t from 1 ms to 100 ms. Each test was repeated five times. For RP-

https://doi.org/10.1021/acsmaterialslett.5c01084
ACS Materials Lett. 2025, 7, 3943−3951

MRs initially magnetized in parallel, the reprogramming success rate as a function of time is plotted in Figure 3b. Three distinct regimes were identified: when the ramp time is shorter than 40 ms, MRs can be successfully reprogrammed, defined as the reprogrammable regime; for $t > 70$ ms, no reprogramming occurred, defined as the non-reprogrammable regime; in the intermediate range ($t = 40-70$ ms), the RP-MR exhibited random behavior—successful in some trials but not in others. We define this as the unstable regime, which corresponds to a transitional state where minor variations in the robot's configuration or environmental conditions can lead to different outcomes. A similar trend was observed for RP-MRs initially magnetized in the antiparallel state (Figure 3e). However, the reprogrammable regime in this case was significantly narrower (1−15 ms). The success of magnetization switching depends on the ramp time of the applied magnetic field. A ramp time of 10 ms allows for rapid remagnetization of the nickel nanowires before the SU-8 panel can physically rotate in response to the changing field, as shown in Figure S2(a). In contrast, a slower ramp time of 100 ms allows the panel to rotate before remagnetization is complete, leading to a failed switch, as shown in Figure S2(b). This is due to the interplay between the magnetic switching speed and the mechanical response time of the SU-8 panels in the fluid environment, which is influenced by the robot's geometry and fluidic drag.

We next explored the relationship between the reprogrammable dynamics and geometric parameters of the RP-MRs. Six configurations with three panel size s (set to 100, 150, and 200 μm) and two hinge length w (set to 100 and 150 μm) were investigated. For each configuration and initial magnetization state (parallel or antiparallel direction), the reprogramming behavior was again categorized into the programmable, unstable, non-programmable regimes. The results are summarized in Figure 3c,f, where orange denotes the reprogrammable regime, gray denotes the unstable regime, and purple denotes the non-reprogrammable regime. For MRs in a parallel magnetization state, the reprogrammable regime expanded with increasing panel size. While the width of the unstable regime remains relatively constant, the onset of the non-reprogrammable regime is delayed. This trend is primarily attributed to the increased inertia and, thus, resistance to rotation for the larger robots, which delays the mechanical realignment under external magnetic fields. In contrast, for robots with antiparallel magnetization state, the reprogrammable regime remains relatively consistent across all sizes. However, the unstable regime becomes narrower with increasing size, and the non-reprogrammable regime shifts slightly toward longer ramp times. Compared with the case with parallel magnetization, these shifts are less pronounced. This behavior can be explained by the stronger mechanical response (i.e., folding) under reversed fields in the antiparallel state, which introduces greater dynamic instability during magnetization.

To demonstrate the universality of the reprogramming method and the diversity of deformation and locomotion modes, we further fabricated a strip-shaped microrobot composed of four magnetic panels. Each adjacent pair of panels contains different types of nickel nanowires (MP A and MP B), all magnetized along the longitudinal axis of the robot. As a result, the robot can exhibit two distinct magnetic configurations: the uniform magnetization state, where the magnetization in all panels is aligned in the parallel direction (Figure 4a), and an alternating magnetization state, where neighboring panels have antiparallel magnetization (Figure 4e). In the uniform state, when an in-plane rotating magnetic field is applied, the robot extends all panels and rotates in place around a fixed point (Figure 4b and Video S3). When subjected to an out-of-plane rotating field, the robot maintains its extended form and rotates along its width direction, producing net displacement (Figure 4c and Video S3). Under an oscillating magnetic field, the robot performs periodic swinging motions of its two outermost panels in a sequential and symmetric manner (Figure 4d and Video S3). When the MR was reprogrammed to the alternating magnetization state, the in-plane rotating magnetic field makes the robot fold into "w"-shape and rotate in place around a point (Figure 4f and Video S3). Under an out-of-plane rotating field, the robot retains the "w"-shape and rolls along its width direction, leading to a net translational motion (Figure 4g and Video S3). When driven by an oscillating magnetic field, the robot performs regular back-and-forth swinging in the "w"-shape (Figure 4h and Video S3). Figure 4 panels i and j, along with Video S4, respectively demonstrate the magnetization switching from the parallel to the antiparallel state and vice versa, confirming the reversibility and generality of the *in situ* magnetic reprogramming strategy. Notably, all motion modes shown in Figure 4 can be repeatedly performed on the same robot in aqueous environments, underscoring the platform's adaptability and high functional diversity. Overall, the RP-MRs fabricated via this method can achieve more than six distinct deformation and locomotion modes (Figure 4b−d,f−h), significantly expanding the functional repertoire of microrobotic systems.

The potential for biological applications of our microrobotic platform warrants a careful consideration of biocompatibility. The nickel nanowires are largely encapsulated within the SU-8 matrix, minimizing direct exposure to biological tissues. SU-8, in its cured state, has demonstrated good biocompatibility in various biomedical applications.[27−29] While nickel toxicity is a valid concern, the small quantity of nickel used in our devices, combined with the SU-8 encapsulation, significantly reduces the risk. Furthermore, localized delivery and controlled actuation minimize the systemic exposure. Nevertheless, further investigations, including in vitro and in vivo studies, are necessary to thoroughly assess the biocompatibility for specific biological applications. Future work will focus on conducting comprehensive biocompatibility assessments tailored to specific target applications.

The multimodal deformation and locomotion capabilities of our magnetic microrobots offer significant advantages for navigating the complex and often challenging environments within biological systems. The ability to switch between distinct modes, such as rolling, flipping, and twisting, allows for an adaptable and efficient movement through diverse terrains and across varying length scales. For instance, a rolling mode might be ideal for traversing relatively smooth surfaces within larger cavities, while a twisting or inchworm-like motion could facilitate navigation through confined, tortuous spaces like blood vessels or the tissue interstitium. Furthermore, the capacity for on-demand shape transformation, enabled by our rapid magnetic reprogramming strategy, allows the microrobot to adapt to changing conditions in real-time. This dynamic adaptability is crucial for effectively bypassing obstacles, navigating constrictions, and accessing targeted locations within complex and heterogeneous landscapes characteristic

https://doi.org/10.1021/acsmaterialslett.5c01084
ACS Materials Lett. 2025, 7, 3943−3951

of biological environments. This versatility in locomotion and deformation significantly enhances the potential of our microrobots for diverse in vivo applications, including targeted drug delivery, minimally invasive surgery, and biopsy procedures.

The fundamental advantage of our approach lies in the seamless integration of magnetic nanowire programming with the high flexibility of photolithography-based microfabrication. This synergy allows for the facile design and realization of microrobots with diverse structural complexities and tailored magnetic properties, moving beyond simplified demonstrators. To underscore this versatility, we have successfully fabricated and demonstrated the reprogramming capability in microrobots featuring intricate designs such as orthogonally arranged magnetized panel arrays, quadrupedal composites, Miura fold arrays, and a variety of specialized structures including striped tail-wings, crawler-types, and windmill-shaped configurations (Supplementary Figure S5 and Figure S6). The ability to produce these complex forms using the same underlying process, simply by adapting mask designs, confirms the robustness and broad applicability of our magnetic reprogramming strategy for a wide spectrum of future microrobot designs.

In this work, we present a reprogrammable magnetic microrobot platform based on the coercivity contrast of nickel nanowires with different diameters embedded in the SU-8. By applying external magnetic fields with tailored amplitude and ramp time, *in situ* switching of magnetization states was achieved, enabling a single microrobot to transition between multiple deformation and locomotion modes under identical actuation fields. Systematic experiments revealed the critical influence of magnetization timing and robot geometry on the reprogramming efficiency. Our quantitative comparisons (Table S1) confirm the superiority of the proposed method in both functional diversity and reprogramming efficiency. Compared to thermal-actuated systems ($\leq$3 modes) and uniformly magnetized robots ($\leq$3 modes), the coercivity-gradient strategy enables six modes while eliminating thermal inertia or structural reconfiguration, achieving millisecond-scale switching speeds (>1000-fold faster than chemical methods). This innovation addresses the critical limitations of functional rigidity and slow response in conventional magnetic robots, demonstrating for the first time a unified platform capable of executing complex locomotion with real-time adaptability.

Looking ahead, the fabrication versatility of our microrobots, which allows for predefined multidirectional magnetic orientations (Supplementary Figure S5), opens avenues for realizing more complex and arbitrary magnetic reprogramming strategies. While our current experimental platform is limited to single-axis field switching, the development of advanced multiaxis magnetic field generation systems will be a key focus for future research. This will enable us to fully exploit the potential for precise, arbitrary magnetic reprogramming and high-precision actuation in microrobots with complexly engineered magnetic panels.

■ ASSOCIATED CONTENT

Supporting Information

The Supporting Information is available free of charge at https://pubs.acs.org/doi/10.1021/acsmaterialslett.5c01084.

Additional details on the design and fabrication of the nickel nanowires and microrobots, materials, and methods, including photographs of experimental setup (PDF)

Motion of microrobot (MP4)

Magnetization results (MP4)

Microrobot with magnetic segments (MP4)

In situ programming (MP4)

■ AUTHOR INFORMATION

Corresponding Authors

Xiang-zhong Chen − *International Institute for Intelligent Nanorobots and Nanosystems & State Key Laboratory of Surface Physics, College of Intelligent Robotics and Advanced Manufacturing and College of Intelligent Robotics and Advanced Manufacturing, Shanghai Frontiers Science Research Base of Intelligent Optoelectronics and Perception, Institute of Optoelectronics, Fudan University, Shanghai 200438, People's Republic of China; Zhejiang Key Laboratory of Extreme Environment Functional Materials, Yiwu Research Insititute of Fudan University, Yiwu 322000, China;* orcid.org/0000-0002-2294-7487; Email: xzchen@fudan.edu.cn

Jizhai Cui − *International Institute for Intelligent Nanorobots and Nanosystems & State Key Laboratory of Surface Physics, College of Intelligent Robotics and Advanced Manufacturing, Fudan University, Shanghai 200438, People's Republic of China; Zhejiang Key Laboratory of Extreme Environment Functional Materials, Yiwu Research Insititute of Fudan University, Yiwu 322000, China;* orcid.org/0000-0003-1317-0570; Email: jzcui@fudan.edu.cn

Authors

Guohonghao Zeng − *International Institute for Intelligent Nanorobots and Nanosystems & State Key Laboratory of Surface Physics, College of Intelligent Robotics and Advanced Manufacturing, Fudan University, Shanghai 200438, People's Republic of China; Zhejiang Key Laboratory of Extreme Environment Functional Materials, Yiwu Research Insititute of Fudan University, Yiwu 322000, China*

Hemin Pan − *International Institute for Intelligent Nanorobots and Nanosystems & State Key Laboratory of Surface Physics, College of Intelligent Robotics and Advanced Manufacturing, Fudan University, Shanghai 200438, People's Republic of China; Zhejiang Key Laboratory of Extreme Environment Functional Materials, Yiwu Research Insititute of Fudan University, Yiwu 322000, China*

Maxim A. Kurochkin − *International Institute for Intelligent Nanorobots and Nanosystems & State Key Laboratory of Surface Physics, College of Intelligent Robotics and Advanced Manufacturing, Fudan University, Shanghai 200438, People's Republic of China; Zhejiang Key Laboratory of Extreme Environment Functional Materials, Yiwu Research Insititute of Fudan University, Yiwu 322000, China*

Yang Zong − *International Institute for Intelligent Nanorobots and Nanosystems & State Key Laboratory of Surface Physics, College of Intelligent Robotics and Advanced Manufacturing, Fudan University, Shanghai 200438, People's Republic of China; Zhejiang Key Laboratory of Extreme Environment Functional Materials, Yiwu Research Insititute of Fudan University, Yiwu 322000, China*

Songyu Xiong − *International Institute for Intelligent Nanorobots and Nanosystems & State Key Laboratory of*

https://doi.org/10.1021/acsmaterialslett.5c01084
ACS Materials Lett. 2025, 7, 3943−3951

Surface Physics, College of Intelligent Robotics and Advanced Manufacturing, Fudan University, Shanghai 200438, People's Republic of China; Zhejiang Key Laboratory of Extreme Environment Functional Materials, Yiwu Research Insititute of Fudan University, Yiwu 322000, China

Jinbo Yang − *International Institute for Intelligent Nanorobots and Nanosystems & State Key Laboratory of Surface Physics, College of Intelligent Robotics and Advanced Manufacturing, Fudan University, Shanghai 200438, People's Republic of China; Zhejiang Key Laboratory of Extreme Environment Functional Materials, Yiwu Research Insititute of Fudan University, Yiwu 322000, China*

Minjie Xi − *International Institute for Intelligent Nanorobots and Nanosystems & State Key Laboratory of Surface Physics, College of Intelligent Robotics and Advanced Manufacturing, Fudan University, Shanghai 200438, People's Republic of China; Zhejiang Key Laboratory of Extreme Environment Functional Materials, Yiwu Research Insititute of Fudan University, Yiwu 322000, China*

Yu Mei − *International Institute for Intelligent Nanorobots and Nanosystems & State Key Laboratory of Surface Physics, College of Intelligent Robotics and Advanced Manufacturing, Fudan University, Shanghai 200438, People's Republic of China; Zhejiang Key Laboratory of Extreme Environment Functional Materials, Yiwu Research Insititute of Fudan University, Yiwu 322000, China*

Yongfeng Mei − *International Institute for Intelligent Nanorobots and Nanosystems & State Key Laboratory of Surface Physics, College of Intelligent Robotics and Advanced Manufacturing and College of Intelligent Robotics and Advanced Manufacturing, Shanghai Frontiers Science Research Base of Intelligent Optoelectronics and Perception, Institute of Optoelectronics, Fudan University, Shanghai 200438, People's Republic of China; Zhejiang Key Laboratory of Extreme Environment Functional Materials, Yiwu Research Insititute of Fudan University, Yiwu 322000, China;* orcid.org/0000-0002-3314-6108

Complete contact information is available at: https://pubs.acs.org/10.1021/acsmaterialslett.5c01084

Author Contributions

[▽]G.Z. and H.P. contributed equally to this work.

Notes

The authors declare no competing financial interest.

■ ACKNOWLEDGMENTS

This work is supported by the National Key Technologies R&D Program of China (2022YFA1207000, 2021YFA0715302), National Natural Science Foundation of China (52101214, 62375054, 52473254), Shanghai Rising-Star Program (24QA2700700), Science and Technology Commission of Shanghai Municipality (24520750200, 24CL2900200) and Shanghai Talent Programs. Part of the experimental work was carried out in the Fudan nanofabrication laboratory.

■ REFERENCES

(1) Zhou, H.; Mayorga-Martinez, C. C.; Pané, S.; et al. Magnetically driven micro and nanorobots. *Chem. Rev.* **2021**, *121*, 4999−5041.

(2) Ergeneman, O.; Chatzipirpiridis, G.; Pokki, J.; et al. In vitro oxygen sensing using intraocular microrobots. *IEEE Transactions on Biomedical Engineering* **2012**, *59*, 3104−3109.

(3) Zhou, H.; Mayorga-Martinez, C. C.; Pumera, M. Microplastic removal and degradation by mussel-inspired adhesive magnetic/enzymatic microrobots. *Small Methods* **2021**, *5*, No. 2100230.

(4) Wu, Z.; Zhang, Y.; Ai, N.; et al. Magnetic mobile microrobots for upstream and downstream navigation in biofluids with variable flow rate. *Advanced Intelligent Systems* **2022**, *4*, No. 2100266.

(5) Schmidt, Christine K.; et al. Engineering microrobots for targeted cancer therapies from a medical perspective. *Nat. Commun.* **2020**, *11*, 5618.

(6) Choi, J.; Hwang, J.; Kim, J.; et al. Recent progress in magnetically actuated micro-robots for targeted delivery of therapeutic agents. *Adv. Healthcare Mater.* **2021**, *10*, No. 2001596.

(7) Kong, X.; Gao, P.; Wang, J.; et al. Advances of medical nanorobots for future cancer treatments. *Journal of Hematology & Oncology* **2023**, *16*, 74.

(8) Cao, Q.; Pan, Y.; Zhang, Y.; et al. A dual-functional capsule robot for drug delivery and tissue biopsy based on magnetic torsion spring technology. *Bio-Design and Manufacturing* **2025**, *8*, 495−510.

(9) Neettiyath, A.; Pumera, M. Micro/Nanorobots for Advanced Light-Based Biosensing and Imaging. *Adv. Funct. Mater.* **2025**, *35*, No. 2415875.

(10) Hou, J.; Liu, H.; Huang, L.; et al. Recent advances in micro/nano-robots for environ-mental pollutant removal: Mechanism, application, and prospect. *Chem. Eng. J.* **2024**, *498*, No. 155135.

(11) Zeeshan, M. A.; Pané, S.; Youn, S. K.; et al. Graphite coating of iron nanowires for na-norobotic applications: synthesis, characterization and magnetic wireless manipula-tion. *Adv. Funct. Mater.* **2013**, *23*, 823−831.

(12) Ma, W.; Wang, H. Magnetically driven motile superhydrophobic sponges for efficient oil removal. *Applied Materials Today* **2019**, *15*, 263−266.

(13) Dong, M.; Wang, X.; Chen, X. Z.; et al. 3D-printed soft magnetoelectric microswim-mers for delivery and differentiation of neuron-like cells. *Adv. Funct. Mater.* **2020**, *30*, No. 1910323.

(14) Chang, S. T.; Paunov, V. N.; Petsev, D. N.; et al. Remotely powered self-propelling par-ticles and micropumps based on miniature diodes. *Nat. Mater.* **2007**, *6*, 235−240.

(15) Loget, G.; Kuhn, A. Electric field-induced chemical locomotion of conducting ob-jects. *Nat. Commun.* **2011**, *2*, 535.

(16) Sridhar, V.; Podjaski, F.; Kröger, J.; et al. Carbon nitride-based light-driven micro-swimmers with intrinsic photocharging ability. *Proc. Natl. Acad. Sci. U. S. A.* **2020**, *117*, 24748−24756.

(17) Pourrahimi, A. M.; Villa, K.; Manzanares Palenzuela, C. L.; et al. Catalytic and light-driven ZnO/Pt Janus nano/micromotors: switching of motion mechanism via interface roughness and defect tailoring at the nanoscale. *Adv. Funct. Mater.* **2019**, *29*, No. 1808678.

(18) Esteban-Fernández de Ávila, B.; Angsantikul, P.; Ramírez-Herrera, D. E.; et al. Hybrid biomembrane-functionalized nanorobots for concurrent removal of pathogenic bacteria and toxins. *Science Robotics* **2018**, *3*, No. eaat0485.

(19) Tu, Y.; Peng, F.; Sui, X.; et al. Self-propelled supramolecular nanomotors with temper-ature-responsive speed regulation. *Nat. Chem.* **2017**, *9*, 480−486.

(20) Cui, J.; Huang, T. Y.; Luo, Z.; et al. Nanomagnetic encoding of shape-morphing mi-cromachines. *Nature* **2019**, *575*, 164−168.

(21) Kim, J.; Chung, S. E.; Choi, S. E.; et al. Programming magnetic anisotropy in polymeric microactuators. *Nat. Mater.* **2011**, *10*, 747−752.

(22) Huang, H. W.; Sakar, M. S.; Petruska, A. J.; et al. Soft micromachines with programma-ble motility and morphology. *Nat. Commun.* **2016**, *7*, No. 12263.

(23) Niu, F.; Xue, Q.; Cao, Q.; et al. Magneto-soft robots based on multi-materials optimizing and heat-assisted in-situ magnetic domains programming[J]. *International Journal of Extreme Manufacturing* **2025**, *7*, No. 055506.

(24) Alapan, Y.; Karacakol, A. C.; Guzelhan, S. N.; et al. Reprogrammable shape morphing of magnetic soft machines. *Science Advances* **2020**, *6*, No. eabc6414.

(25) Smart, C. L.; Pearson, T. G.; Liang, Z.; et al. Magnetically programmed diffractive ro-botics. *Science* **2024**, *386*, 1031−1037.
(26) Zong, Y.; Xi, M.; Wang, Y.; et al. Waveguide microactuators self-rolled around an optical fiber taper. *Adv. Mater.* **2025**, *37*, No. 2418316.
(27) Li, J.; Fan, L.; Li, Y.; et al. Development of cell-carrying magnetic microrobots with bioactive nanostructured titanate surface for enhanced cell adhesion. *Micromachines* **2021**, *12*, 1572.
(28) Altuna, A.; Bellistri, E.; Cid, E.; et al. SU-8 based microprobes for simultaneous neural depth recording and drug delivery in the brain. *Lab Chip* **2013**, *13*, 1422−1430.
(29) Ye, J.; Wilson, D. A.; Tu, Y.; et al. 3D-Printed Micromotors for Biomedical Applications. *Advanced Materials Technologies* **2020**, *5*, No. 2000435.

https://doi.org/10.1021/acsmaterialslett.5c01084
ACS Materials Lett. 2025, 7, 3943−3951